JOURNAL OF GUIDANCE, CONTROL, AND DYNAMICS
Vol. 32, No. 3, May–June 2009

Terminal-Area Aircraft Tracking Using Hybrid Estimation

Chze Eng Seah* and Inseok Hwang†
Purdue University, West Lafayette, Indiana 47907

DOI: 10.2514/1.40127

A bottleneck to the flow of air traffic is in the traffic around airports. Accurate tracking of aircraft movements around airports is important to improve traffic capacity and safety. We propose a hybrid estimation algorithm that uses the knowledge of departure or arrival aircraft flight plans and nominal flight profiles to improve tracking of aircraft movements around airports. The algorithm also provides an accurate estimation of aircraft flight modes that is often used in conflict detection, intent inference, and trajectory prediction algorithms. In the algorithm, we first develop a methodology to model flight mode transitions based on typical aircraft landing profiles, takeoff profiles, and standard flight routes around airports. Based on the model, we derive a conditional mode transition matrix that is dependent (or conditioned) on the continuous state of the aircraft. The aircraft-tracking problem is then solved using a hybrid estimation algorithm. We also present an analytical result that reduces the dimension, and hence the computational cost, of a multivariate integral that arises due to the continuous-state-dependent mode transition matrix. We present two simulation examples to illustrate the performance of our aircraft-tracking algorithm.

Nomenclature

$\mathcal{A}, \mathcal{B}$	=	logical statements
A, B, C, D	=	state matrices
$\mathcal{C}$	=	logical statement describing the guard condition (or mode transitions)
d	=	distance
h	=	aircraft's altitude
$\mathcal{I}$	=	logical true
k	=	discrete time
L_x, L_θ	=	constant matrices that describe guard conditions
M^k	=	set of mode histories up to time k
m	=	aircraft's flight mode
$\mathcal{N}_q(\cdot)$	=	q-dimensional Gaussian probability density function
P	=	covariance of the continuous-state estimate
Q	=	process noise covariance
R	=	measurement noise covariance
T_s	=	sampling interval
v	=	aircraft's speed
w	=	process noise
x	=	continuous state, $\mathbb{R}^n$
$\hat{x}$	=	mean of the continuous-state estimate
Z^k	=	set of measurements up to time k
z	=	measurement vector
θ	=	q-dimensional vector with multivariate Gaussian probability density function
μ	=	mean of Gaussian probability distribution
ν	=	measurement noise
ξ, η	=	aircraft's coordinates in horizontal plane
Π	=	continuous-state-dependent mode transition matrix
π_{ij}	=	continuous-state-dependent mode transition probability
Σ	=	Covariance of Gaussian probability distribution
$\Phi_q(\cdot)$	=	q-dimensional Gaussian cumulative density function
ψ	=	aircraft's heading
$\wedge$	=	logical and
$\vee$	=	logical or
$\oslash$	=	logical false

Subscripts

i	=	aircraft's flight mode at time k
j	=	aircraft's flight mode at time $k+1$

Presented as Paper 6691 at the AIAA Guidance, Navigation, and Control Conference and Exhibit, Hilton Head, SC, 20–23 August 2007; received 29 July 2008; revision received 19 November 2008; accepted for publication 20 November 2008.

*Graduate Student, School of Aeronautics and Astronautics; seah@purdue.edu.

†Assistant Professor, School of Aeronautics and Astronautics; ihwang@purdue.edu. Member AIAA.

I. Introduction

AIR Traffic Control (ATC) is responsible for managing the flow of aircraft operating within the National Airspace System. The Federal Aviation Administration has projected that demands at the nation's major airports may exceed capacity for several years to come [1]. Hence, the flow of traffic around airports is a major bottleneck to air traffic. Various researchers have investigated several concepts to enhance future air traffic management. These include conflict detection and resolution [2–7], pilot intent inference [8,9], accurate aircraft trajectory predictions [10], and aircraft time-of-arrival predictions [11]. A key requirement for implementation of the preceding concepts is an accurate knowledge of aircraft positions, velocities, and flight modes. Furthermore, an accurate modeling of aircraft flight mode transitions is required for conformance monitoring under future air traffic management operations (such as airborne spacing, trajectory-based operations, and superdensity operations) under the Next Generation Air Transportation System (NextGen) [12]. In this paper, we propose a hybrid system for modeling aircraft dynamics and flight mode transitions in terminal areas (TRACON) and propose a corresponding hybrid estimation algorithm for accurate tracking of aircraft positions and estimation of flight modes.

Hybrid estimation (or multiple-model) algorithms have been used in many target-tracking applications, including air traffic surveillance [13,14]. In these applications, aircraft dynamics are divided into a number of flight modes (or discrete states), such as constant velocity, coordinated turn, constant descent, etc. In each flight mode, the aircraft dynamics are then described by simpler, possibly linear, dynamic equations. Hybrid estimation algorithms are able to achieve superior performance by using different state estimators matched to the aircraft dynamics for different flight modes. The performance of a hybrid estimation algorithm hence depends greatly on timely and accurate detection of flight mode transitions [13,15].

Many hybrid estimation algorithms model the mode transitions as a Markov process with a constant mode transition matrix, independent of the continuous-state variables [13]. However, this is not the case in ATC tracking applications, especially for aircraft tracking in the TRACON. To ensure the safety of the flight and to facilitate the management of air traffic, the standard route structures around the airport, such as standard instrument departure (SID) and standard terminal arrival routes (STARs), are imposed [16]. Furthermore, the intent information of the aircraft is filed in the flight plan, which consists of segments within the fixed route structure. For example, Fig. 1 shows the STARs into Memphis International Airport. Because an arrival aircraft typically follows one of the STARs, the flight mode of the aircraft depends on its position with respect to the intended arrival route. Thus, with information provided by the filed flight plan, it is possible to model the flight mode transition probabilities of the aircraft as being dependent on the state of the aircraft, such as its position.

A popular approach for hybrid estimation is based on multiple-model Kalman filters. Algorithms based on this approach, such as the interacting multiple-model (IMM) algorithm, have been shown to give excellent performance with low computational cost [13,17]. However, the IMM algorithm and other similar algorithms based on this approach usually assume constant mode transition probabilities. An alternative approach is based on particle filters [18,19] which use random samples (or particles) to represent the probability distribution of the state estimation. These simulation-based algorithms perform well in nonlinear estimation problems, but they generally have high computational costs [19].

In this paper, we use a multiple-model Kalman filter algorithm [20] for aircraft tracking. However, unlike other multiple-model Kalman filter algorithms, our algorithm considers mode transition probabilities to be dependent on the continuous state, such as position and velocity, of the aircraft. In the algorithm, we first propose a methodology for modeling the flight mode transitions of aircraft movements around airports. We consider typical aircraft landing profiles, aircraft takeoff profiles, and aircraft movements along SIDs/STARs. Based on the model, we derive a conditional mode transition matrix that is dependent (or conditioned) on the continuous state of the aircraft. The aircraft-tracking problem is then solved using a hybrid estimation algorithm, which has been proposed in the authors' previous work [20], that uses continuous-state-dependent mode transition matrix.

In the authors' previous work [20], we used a Monte Carlo integration method to evaluate the mode transition probabilities, which are given as multivariate integrals. In this paper, we propose an analytical result that reduces the multivariate integrals into multivariate Gaussian cumulative density functions (cdf). Although, in general, the multivariate Gaussian cdf is also a multivariate integral that needs to be evaluated numerically, the analytical result reduces the dimension of this integration and thus reduces its computational cost. We illustrate the performance of our aircraft-tracking algorithm with two illustrative examples. The simulation results show that the proposed algorithm yields better tracking accuracy and mode-estimation accuracy, with only a small increase in computational time, compared with various designs of the IMM algorithm.

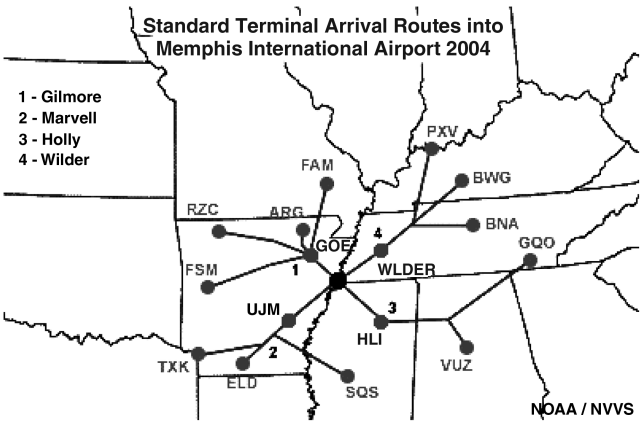

Fig. 1 Four main STARs used for Memphis International Airport. Note that navigation aids (VOR/DME) are indicated by three-letter identifiers, and arrival gates are typically given full names (e.g., Gilmore). Airline dispatch departments file flight plans using these STARs.

This paper is organized as follows: Sec. II presents a stochastic linear hybrid-system model of the aircraft dynamics and a methodology to model the mode transitions. Sec. III presents a corresponding hybrid estimation algorithm for aircraft tracking. In the algorithm, we also present an analytical result to reduce the computational cost of evaluating the mode transition probabilities. In Sec. IV, we illustrate the performance of the algorithm with simulations. Conclusions are presented in Sec. V.

II. Aircraft Model

A. Aircraft Dynamics and Measurement Model

We consider the behavior of an aircraft in a local navigation frame with the ξ axis pointing east, the η axis pointing north, and the h axis pointing up. Let

$$x = [\xi \quad \dot{\xi} \quad \ddot{\xi} \quad \eta \quad \dot{\eta} \quad \ddot{\eta} \quad h \quad \dot{h}]^T$$

be the continuous-state vector. In our aircraft model, the dynamics of the aircraft in the horizontal plane (i.e., ξ–η plane) is independent of that in the vertical plane. Hence, we divide the aircraft dynamics into a number of submodes in both the horizontal plane and the vertical plane. The various submodes are subsequently described qualitatively. The dynamics of the aircraft in each submode will be subsequently discussed.

1. *Horizontal-Flight Submodes*

1) At constant velocity (CV), the aircraft moves at a constant speed and heading.

2) At constant acceleration/deceleration (CA), the aircraft increases or decreases speed while maintaining a constant heading. This mode usually corresponds to takeoff or landing conditions and may sometimes correspond to conflict-resolution scenarios.

3) In a coordinated turn (CT), the aircraft takes a heading change by turning at a constant speed and constant turning rate.

2. *Vertical-Flight Submodes*

1) At constant height (CH), the aircraft moves with no or little change in height (or altitude), corresponding to level flight.

2) In a constant descent/climb (CD): the aircraft descends or climbs at a constant altitude change rate. This mode typically corresponds to landing or takeoff conditions.

The mode of an aircraft at any time is characterized by a combination of submodes in each plane. For example, the mode of the aircraft is (CV, CH) if the aircraft is moving at constant speed and constant altitude. Thus, the total number of modes in the aircraft model is six.

To describe the aircraft dynamics in each submode, we let $x = [x_l \quad x_v]^T$, where

$$x_l = [\xi \quad \dot{\xi} \quad \ddot{\xi} \quad \eta \quad \dot{\eta} \quad \ddot{\eta}]^T$$

and $x_v = [h \quad \dot{h}]^T$. The aircraft dynamics in each submode are described next.

3. *Lateral Dynamics in the Horizontal Plane*

a. CV Mode. In the CV mode, we model the aircraft acceleration as a white Gaussian noise. The aircraft dynamics are described by

$$x_l(k+1) = \begin{bmatrix} 1 & T_s & 0 & 0 & 0 & 0 \\ 0 & 1 & 0 & 0 & 0 & 0 \\ 0 & 0 & 0 & 0 & 0 & 0 \\ 0 & 0 & 0 & 1 & T_s & 0 \\ 0 & 0 & 0 & 0 & 1 & 0 \\ 0 & 0 & 0 & 0 & 0 & 0 \end{bmatrix} x_l(k) + \begin{bmatrix} \frac{T_s^2}{2} & 0 \\ T_s & 0 \\ 1 & 0 \\ 0 & \frac{T_s^2}{2} \\ 0 & T_s \\ 0 & 1 \end{bmatrix} \begin{bmatrix} w_{\xi_{\mathrm{CV}}} \\ w_{\eta_{\mathrm{CV}}} \end{bmatrix} \tag{1}$$

where T_s is the sampling interval, and $w_{\xi_{\mathrm{CV}}}$ and $w_{\eta_{\mathrm{CV}}}$ are white Gaussian noise with mean zero and covariance:

$$Q_{\mathrm{CV}} = \begin{bmatrix} E[w_{\xi_{\mathrm{CV}}}^2] & 0 \\ 0 & E[w_{\eta_{\mathrm{CV}}}^2] \end{bmatrix} = \begin{bmatrix} 0.5^2 & 0 \\ 0 & 0.5^2 \end{bmatrix} (\mathrm{m/s^2})^2 \tag{2}$$

The covariance Q_{CV} and the covariance for the other flight modes are design parameters. Here, we have chosen the covariance by tuning the Kalman filter performance based on simulations.

b. CT Mode. In the CT mode, we use a Wiener-sequence acceleration model given by

$$x_l(k+1) = \begin{bmatrix} 1 & T_s & \frac{T_s^2}{2} & 0 & 0 & 0 \\ 0 & 1 & T_s & 0 & 0 & 0 \\ 0 & 0 & 1 & 0 & 0 & 0 \\ 0 & 0 & 0 & 1 & T_s & \frac{T_s^2}{2} \\ 0 & 0 & 0 & 0 & 1 & T_s \\ 0 & 0 & 0 & 0 & 0 & 1 \end{bmatrix} x_l(k) + \begin{bmatrix} \frac{T_s^2}{2} & 0 \\ T_s & 0 \\ 1 & 0 \\ 0 & \frac{T_s^2}{2} \\ 0 & T_s \\ 0 & 1 \end{bmatrix} \begin{bmatrix} w_{\xi_{\mathrm{CT}}} \\ w_{\eta_{\mathrm{CT}}} \end{bmatrix} \tag{3}$$

where $w_{\xi_{\mathrm{CT}}}$ and $w_{\eta_{\mathrm{CT}}}$ are, respectively, white Gaussian white noise with mean zero and covariance:

$$Q_{\mathrm{CT}} = \begin{bmatrix} E[w_{\xi_{\mathrm{CT}}}^2] & 0 \\ 0 & E[w_{\eta_{\mathrm{CT}}}^2] \end{bmatrix} = \begin{bmatrix} 10^2 & 0 \\ 0 & 10^2 \end{bmatrix} (\mathrm{m/s^2})^2 \tag{4}$$

c. CA Mode. In the CA mode, the same Wiener-sequence acceleration model as that in the CT mode is used. The difference between the CA and CT modes is in the noise covariance. In the CA mode, the aircraft speed changes, but the heading remains constant. Hence, we model the noise covariance of the CA mode to be large in the direction parallel to the aircraft's heading and small in the direction perpendicular to the aircraft's heading. The process noise covariance in the CA mode is

$$\begin{aligned} Q_{\mathrm{CA}} &= \begin{bmatrix} E[w_{\xi_{\mathrm{CA}}}^2] & 0 \\ 0 & E[w_{\eta_{\mathrm{CA}}}^2] \end{bmatrix} \\ &= \begin{bmatrix} \{5\cos(\psi(k))\}^2 & 0 \\ 0 & \{5\sin(\psi(k))\}^2 \end{bmatrix} (\mathrm{m/s^2})^2 \end{aligned} \tag{5}$$

where

$$\psi(k) = \arctan\left(\frac{\dot{\xi}(k)}{\dot{\eta}(k)}\right)$$

is the heading of the aircraft.

4. Longitudinal Dynamics in the Vertical Plane

a. CH Mode. In the CH mode, the aircraft's altitude is almost constant. The aircraft dynamics are modeled as

$$x_v(k+1) = \begin{bmatrix} 1 & 0 \\ 0 & 0 \end{bmatrix} x_v(k) + \begin{bmatrix} T_s \\ 0 \end{bmatrix} w_{\mathrm{CH}} \tag{6}$$

where w_{CH} is a white Gaussian noise with mean zero and covariance

$$Q_{\mathrm{CH}} = E[w_{\mathrm{CH}}^2] = 0.25^2 \ (\mathrm{m/s})^2 \tag{7}$$

b. CD Mode. In the CD mode, the rate of change aircraft's height is almost constant. The aircraft dynamics are modeled as

$$x_v(k+1) = \begin{bmatrix} 1 & T_s \\ 0 & 1 \end{bmatrix} x_v(k) + \begin{bmatrix} T_s \\ 1 \end{bmatrix} w_{\mathrm{CD}} \tag{8}$$

where w_{CD} is a white Gaussian noise with mean zero and covariance:

$$Q_{\mathrm{CD}} = E[w_{\mathrm{CD}}^2] = 0.5^2 \ (\mathrm{m/s})^2 \tag{9}$$

5. Measurement Model

It is assumed that the measurements are taken from a surveillance radar, which gives the position of the aircraft at 5 s intervals [14]. Radar measurements are usually reported in polar coordinates and the accuracy depends on the distance of an aircraft from the radar. In our simulations presented in Sec. IV, we assume that the radar measurements are converted to the ξ, η, and h coordinates (the local navigation frame), and the standard deviation of measurement noise is 100 m ($\approx$300 ft) in each axis [14]. Thus, although the actual radar measurement model is nonlinear/non-Gaussian, it can be approximated by a linear model given by [14]

$$z(k) = \begin{bmatrix} 1 & 0 & 0 & 0 & 0 & 0 & 0 & 0 \\ 0 & 0 & 0 & 1 & 0 & 0 & 0 & 0 \\ 0 & 0 & 0 & 0 & 0 & 0 & 1 & 0 \end{bmatrix} x(k) + \begin{bmatrix} \nu_\xi(k) \\ \nu_\eta(k) \\ \nu_h(k) \end{bmatrix} \tag{10}$$

where $z(k)$ is the measured position vector, and $\nu_\xi(k)$, $\nu_\eta(k)$, and $\nu_h(k)$ are Gaussian noise with mean zero and covariance:

$$R = \begin{bmatrix} E[\nu_\xi^2] & 0 & 0 \\ 0 & E[\nu_\eta^2] & 0 \\ 0 & 0 & E[\nu_h^2] \end{bmatrix} = \begin{bmatrix} 100^2 & 0 & 0 \\ 0 & 100^2 & 0 \\ 0 & 0 & 100^2 \end{bmatrix} (\mathrm{m^2}) \tag{11}$$

B. Flight-Mode Transitions: Deterministic Model

Now we want to develop a mathematical model to describe the mode transitions of the aircraft dynamics. We will derive a stochastic model that describes the probabilities of mode transitions as functions of the continuous state of the aircraft. We do this in two steps. First, in this section, we model the mode transitions by assuming that the flight profile of a departure or an arrival aircraft is known. This will lead us to a deterministic model that clearly defines the conditions under which various mode transitions occur. In the next section, we will then extend this deterministic model to a stochastic model that takes into consideration the probabilistic variations of aircraft flight profiles in actual applications. The flight profiles considered are as follows: 1) aircraft takeoff profile, 2) aircraft landing profile, and 3) aircraft movement along SID/STAR.

1. Aircraft Takeoff Profile

Figure 2 illustrates a typical takeoff profile of a Boeing B747-200 aircraft [21]. The aircraft dynamics are divided into the various submodes discussed in Sec. II.A. It can be seen that submode transitions (and thus mode transitions) occur at various points along the given flight profile. We denote these points along the aircraft flight profile as the *flight mode change points* (FCPs). At each FCP, we develop a model to describe the submode (and mode) transitions.

At this point, we would like to introduce some notation. We use the letters $\mathcal{A}$, $\mathcal{B}$, and $\mathcal{C}$ to denote logical statements. $\mathcal{A} \vee \mathcal{B}$ denotes the case in which either $\mathcal{A}$ is true or $\mathcal{B}$ is true (or both), $\mathcal{A} \wedge \mathcal{B}$ denotes the case in which both $\mathcal{A}$ and $\mathcal{B}$ are true, and $\neg\mathcal{A}$ denotes the case in which $\mathcal{A}$ is not true (or negation of $\mathcal{A}$). $\mathcal{I}$ denotes a logical true and $\oslash$ denotes a logical false. For example, we have $\mathcal{I} \wedge \mathcal{A} = \mathcal{A}$ and $\oslash \vee \mathcal{A} = \mathcal{A}$ for all $\mathcal{A}$.

To illustrate the concept of FCP, let us consider the takeoff profile of an aircraft shown in Fig. 3 and the mode transition model shown in Fig. 4. Let h be the altitude of aircraft and v be the speed of the aircraft given by

$$v = \cos(\psi)\dot{\xi} + \sin(\psi)\dot{\eta} \tag{12}$$

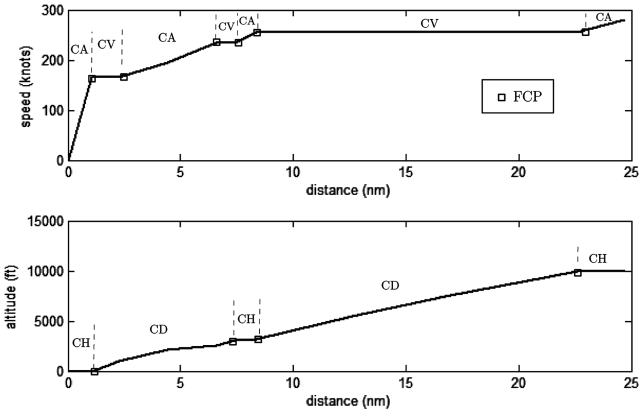

Fig. 2 Typical takeoff profile of a Boeing B747-200 aircraft [21].

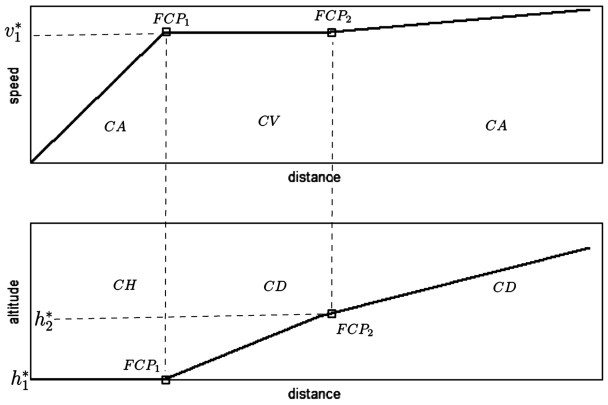

Fig. 3 Initial takeoff profile of a generic aircraft.

where ψ is the heading of the aircraft. For an aircraft landing or taking off, its heading may be taken as the direction of the runway. Initially, the aircraft starts at speed $v = 0$ and height $h = h_1^*$ (see Fig. 3). It first accelerates along the runway [i.e., (CA, CH) mode] and is approaching FCP_1. When the aircraft speed reaches v_1^*, it starts to climb at a constant speed [(CV, CD) mode]. Thus, when the aircraft is approaching FCP_1, we model that the aircraft is in the (CV, CD) mode if $h > h_1^*$ or $v > v_1^*$.

We use the model shown in Fig. 4a to represent the submode transitions in the horizontal plane. In this model, if the statement, or guard condition, $\mathcal{C} = (v > v_1^*) \vee (h > h_1^*)$ is true, the aircraft is in the CV submode in the horizontal plane; otherwise (i.e., if $\neg C$), the aircraft is in the CA submode. There are no conditions that allow the submode to be in CT. This is represented by a logical false $\oslash$. The model for submode transitions in the vertical plane is similarly constructed and is shown in 4b. We defined the mode of the system to be a combination of the horizontal submode and the vertical submode. Hence, the guard conditions for the mode transitions can be derived from that of the submode transition models given in Figs. 4a and 4b. For example, if the guard condition for the horizontal submode transition CA $\rightarrow$ CV is $\mathcal{A}$ and the guard condition for the vertical submode transition CH $\rightarrow$ CD is $\mathcal{B}$, then the guard condition for the mode transition (CA, CH) $\rightarrow$ (CV, CD) is $\mathcal{A} \wedge \mathcal{B}$, and the condition for the mode transition (CA, CH) $\rightarrow$ (CV, CH) is $\mathcal{A} \wedge \neg\mathcal{B}$, etc. Thus, Figs. 4a and 4b completely characterize the mode transition process.

Now let us consider a general structure of the flight mode transition model as shown in Fig. 5. We enumerate the submodes CV, CT, CA, CH, and CD as submodes 1, 2, 3, 4, and 5, respectively. Each guard condition that determines the mode transition from submode i to submode j $(i, j \in \{1, \ldots, 5\})$ is denoted as $\mathcal{C}_{ij}$. The flight mode transition model in Fig. 4 can be described by this general structure with $\mathcal{C}_{31} = \mathcal{C}$ and $\mathcal{C}_{13} = \neg\mathcal{C}$. Note that by de Morgan's law, we have

$$\neg C = \neg((v > v_1^*) \vee (h > h_1^*)) = (v \leq v_1^*) \wedge (h \leq h_1^*)$$

Using Eq. (12), the guard condition $\mathcal{C}_{13}$ can be described by a vector inequality:

$$L_x x + L_\theta \theta^* \leq 0 \tag{13}$$

where

$$L_x = \begin{bmatrix} 0 & \cos(\psi) & 0 & 0 & \sin(\psi) & 0 & 0 & 0 \\ 0 & 0 & 0 & 0 & 0 & 0 & 1 & 0 \end{bmatrix}$$

$$L_\theta = \begin{bmatrix} -1 & 0 \\ 0 & -1 \end{bmatrix}$$

and

$$\theta^* = \begin{bmatrix} v_1^* \\ h_1^* \end{bmatrix}$$

The vector inequality $y \leq 0$ means that each component of the vector y is nonpositive.

Using the general structure of the flight mode transition model, it is sufficient to specify the set of guard conditions $\mathcal{S} = \{\mathcal{C}_{ij} | i, j = 1, \ldots, 5\}$ to describe the flight mode transitions at any FCP. For

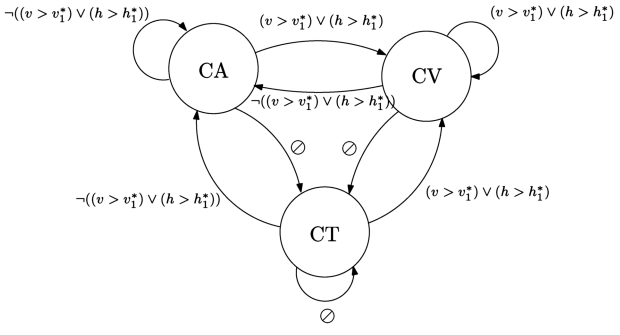

a) Lateral-plane submode transitions

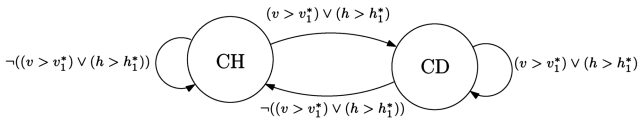

b) Vertical-plane submode transitions

Fig. 4 Flight mode transition model for FCP_1.

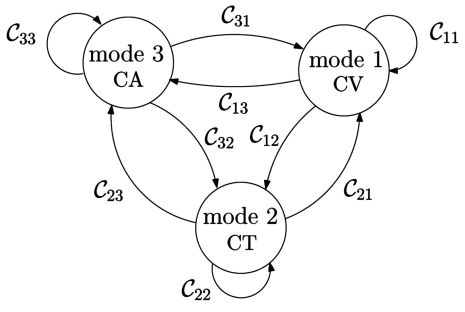

a) Lateral-plane submode transitions

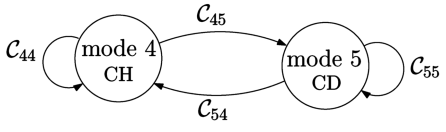

b) Vertical-plane submode transitions

Fig. 5 General structure of flight mode transition model.

Table 1 Set of guard conditions for FCP_1

$$\mathcal{C}_{11} = \mathcal{C}_{21} = \mathcal{C}_{31} = \neg\mathcal{C}_{13}$$
$$\mathcal{C}_{12} = \mathcal{C}_{22} = \mathcal{C}_{32} = \oslash$$
$$\mathcal{C}_{13} = \mathcal{C}_{23} = \mathcal{C}_{33} = L_x x + L_\theta \theta^* \le 0$$
$$\mathcal{C}_{44} = \mathcal{C}_{54} = \neg\mathcal{C}_{13}$$
$$\mathcal{C}_{45} = \mathcal{C}_{55} = \mathcal{C}_{13}$$
$$L_x = \begin{bmatrix} 0 & \cos(\psi) & 0 & 0 & \sin(\psi) & 0 & 0 & 0 \\ 0 & 0 & 0 & 0 & 0 & 0 & 1 & 0 \end{bmatrix}$$
$$L_\theta = \begin{bmatrix} -1 & 0 \\ 0 & -1 \end{bmatrix}$$
$$\theta^* = \begin{bmatrix} v_1^* \\ h_1^* \end{bmatrix}$$

Table 2 Set of guard conditions for FCP_2

$$\mathcal{C}_{11} = \mathcal{C}_{21} = \mathcal{C}_{31} = L_x x + L_\theta \theta^* \le 0$$
$$\mathcal{C}_{12} = \mathcal{C}_{22} = \mathcal{C}_{32} = \oslash$$
$$\mathcal{C}_{13} = \mathcal{C}_{23} = \mathcal{C}_{33} = \neg\mathcal{C}_{31}$$
$$\mathcal{C}_{44} = \mathcal{C}_{54} = \oslash$$
$$\mathcal{C}_{45} = \mathcal{C}_{55} = \mathcal{I}$$
$$L_x = [0 \quad 0 \quad 0 \quad 0 \quad 0 \quad 0 \quad 1 \quad 0]$$
$$L_\theta = -1$$
$$\theta^* = h_2^*$$

example, the set of guard conditions for FCP_1, which is equivalent to the flight mode transition model in Fig. 4, are given in Table 1.

After the aircraft has passed FCP_1, we consider the flight mode transition model for the next FCP, or FCP_2. Here, the submode in the horizontal plane is CA if $h > h_2^*$ and is CV otherwise. The submode in the vertical plane is always CD. The corresponding set of guard conditions for FCP_2 is given in Table 2.

By the preceding process, the entire nominal takeoff profile of the aircraft is modeled as consisting of a set of FCPs, and a flight mode transition model (or equivalently a set of guard conditions $\mathcal{S}$) is formulated for each FCP. Next, we shall see that this concept may also be applied to an aircraft landing profile and a flight profile along SID/STAR.

2. Aircraft Landing Profile

Figure 6 shows a typical landing profile of a Boeing B727 aircraft [22]. Various FCPs have been marked along the given profile. We shall derive the mode transition model for FCP_3 and FCP_4. As illustrated in Fig. 7, we define the distance d_s as

$$d_s = (\xi - \xi_{\text{ref}})\cos(\beta) + (\eta - \eta_{\text{ref}})\sin(\beta) \tag{14}$$

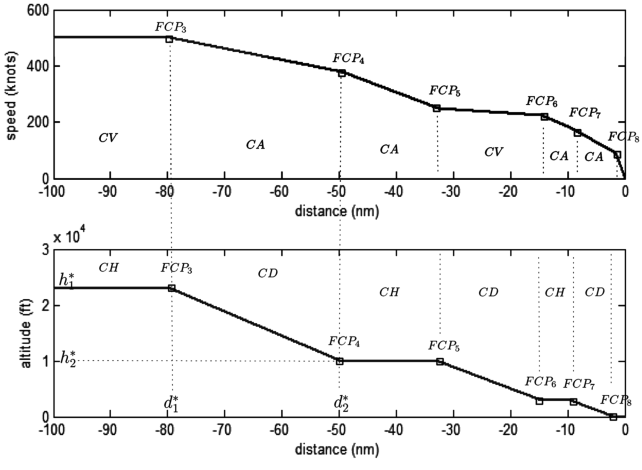

Fig. 6 Typical landing profile of a Boeing 727 aircraft [22].

Table 3 Set of guard conditions for FCP_3

$$\mathcal{C}_{11} = \mathcal{C}_{21} = \mathcal{C}_{31} = L_x x + L_\theta \theta^* \le 0$$
$$\mathcal{C}_{12} = \mathcal{C}_{22} = \mathcal{C}_{32} = \oslash$$
$$\mathcal{C}_{13} = \mathcal{C}_{23} = \mathcal{C}_{33} = \neg\mathcal{C}_{31}$$
$$\mathcal{C}_{44} = \mathcal{C}_{54} = \mathcal{C}_{13}$$
$$\mathcal{C}_{45} = \mathcal{C}_{55} = \neg\mathcal{C}_{13}$$
$$L_x = \begin{bmatrix} -\cos(\beta) & 0 & 0 & -\sin(\beta) & 0 & 0 & 0 & 0 \\ 0 & 0 & 0 & 0 & 0 & 0 & -1 & 0 \end{bmatrix}$$
$$L_\theta = \begin{bmatrix} 1 & 0 \\ 0 & 1 \end{bmatrix}$$
$$\theta^* = \begin{bmatrix} d_1^* + \xi_{\text{ref}}\cos(\beta) + \eta_{ref}\sin(\beta) \\ h_1^* \end{bmatrix}$$

Table 4 Set of guard conditions for FCP_4

$$\mathcal{C}_{11} = \mathcal{C}_{21} = \mathcal{C}_{31} = \oslash$$
$$\mathcal{C}_{12} = \mathcal{C}_{22} = \mathcal{C}_{32} = \oslash$$
$$\mathcal{C}_{13} = \mathcal{C}_{23} = \mathcal{C}_{33} = \mathcal{I}$$
$$\mathcal{C}_{44} = \mathcal{C}_{54} = \neg\mathcal{C}_{45}$$
$$\mathcal{C}_{45} = \mathcal{C}_{55} = L_x x + L_\theta \theta^* \le 0$$
$$L_x = \begin{bmatrix} 0 & -\cos(\psi) & 0 & 0 & -\sin(\psi) & 0 & 0 & 0 \\ 0 & 0 & 0 & 0 & 0 & 0 & -1 & 0 \end{bmatrix}$$
$$L_\theta = \begin{bmatrix} 1 & 0 \\ 0 & 1 \end{bmatrix}$$
$$\theta^* = \begin{bmatrix} d_2^* + \xi_{\text{ref}}\cos(\beta) + \eta_{\text{ref}}\sin(\beta) \\ h_2^* \end{bmatrix}$$

where ξ_{ref}, η_{ref}, and h_{ref} are the coordinates of a reference point (the end of the runway), and β is the runway direction. For FCP_3, we model that the flight mode changes from (CV, CH) to (CA, CD) when $(d_s < d_1^*) \vee (h < h_1^*)$, and it remains in (CV, CH) mode when $(d_s \ge d_1^*) \wedge (h \ge h_1^*)$. For FCP_4, we model that the flight mode changes from (CA, CD) to (CA, CH) when $(d_s < d_2^*) \vee (h < h_2^*)$, and it remains in (CA, CD) mode when $(d_s \ge d_2^*) \vee (h \ge h_2^*)$. The guard conditions corresponding to FCP_3 and FCP_4 are then formulated as given in Tables 3 and 4, respectively.

3. Aircraft Movement Along SID/STAR

Here, we assume that an aircraft is following a standard flight route. An example is given in Fig. 8, which shows a standard route with two straight legs intersecting at a waypoint W_p. Along the standard flight route, the aircraft would start to turn [which corresponds to flight mode transition $(\text{CV}, \text{CH}) \rightarrow (\text{CT}, \text{CH})$] at FCP_{10}, and complete the turn [which corresponds to flight mode transition $(\text{CT}, \text{CH}) \rightarrow (\text{CV}, \text{CH})$] at FCP_{11}. We define the distance d_{s1} to be the distance of the aircraft from W_p projected along the direction of the first leg β_1. Similar to Eq. (14), the distance is given by

$$d_{s1} = (\xi - \xi_{\text{ref}})\cos(\beta_1) + (\eta - \eta_{\text{ref}})\sin(\beta_1) \tag{15}$$

where ξ_{ref} and η_{ref} are the coordinates of W_p. We let d_1^* be the distance of FCP_{10} from W_p along the direction β_1. Then the aircraft

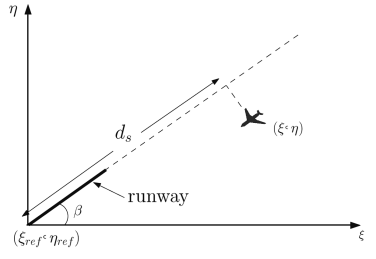

Fig. 7 Definition of distance d_s.

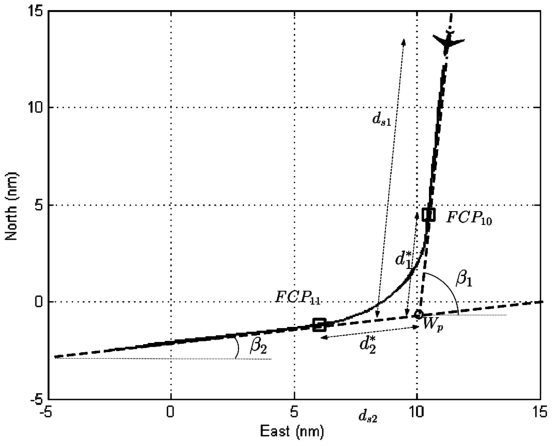

Fig. 8 Aircraft moving along a standard flight route.

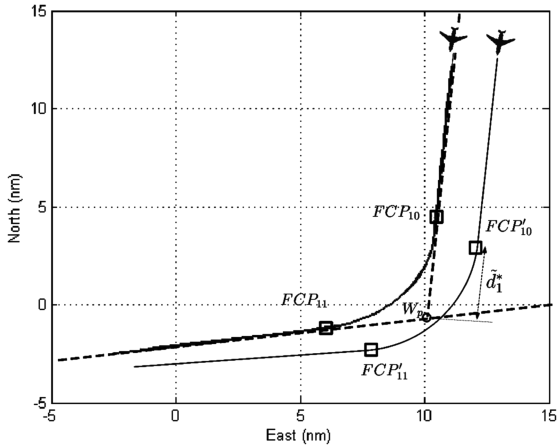

Fig. 9 Aircraft moving along a standard flight route.

would start to turn when the guard condition $d_{s1} \le d_1^*$ is satisfied. The set of guard conditions for FCP_{10} is given in Table 5.

Similarly, we define the distance d_{s2} as the distance of the aircraft from W_p projected along the direction of the second leg β_2, and we define d_2^* as the distance of FCP_{11} from W_p along the direction β_2. The set of guard conditions for FCP_{11} is given in Table 6.

C. Flight-Mode Transitions: Stochastic Model

In this section, we consider the variations in aircraft flight profiles in actual applications. Let us consider the previous example of an aircraft moving along a standard flight route shown in Fig. 8 and the corresponding mode transition model. From Table 5, the mode transition $(\text{CV}, \text{CH}) \to (\text{CT}, \text{CH})$ is governed by the guard condition $d_{s1} \le d_1^*$, which can be written into the general form

$$L_x x + L_\theta \theta^* \le 0 \tag{16}$$

where, in this case,

$$L_x = [\cos(\beta_1) \quad 0 \quad 0 \quad \sin(\beta_1) \quad 0 \quad 0 \quad 0 \quad 0]$$

$L_\theta = -1$, and

$$\theta^* = d_1^* + \xi_{\text{ref}} \cos(\beta_1) + \eta_{\text{ref}} \sin(\beta_1)$$

Figure 9 shows a typical flight profile of the aircraft in practice. The mode transition $(\text{CV}, \text{CH}) \to (\text{CT}, \text{CH})$ is modeled as being governed by guard condition $d_{s1} < \tilde{d}_1^*$, where $\tilde{d}_1^*$ is the distance of FCP'_{10} from W_p, as illustrated. The point FCP'_{10} deviates randomly from the nominal one (FCP_{10}), due to navigation uncertainty. To account for this uncertainty, we consider the parameter d_1^* (and $\tilde{d}_1^*$) in the guard condition to be a random variable. The probability distribution d_1^* may be specified, for example, based on a sample of actual flight profiles. Thus, in general, we consider the parameter θ^* in the guard condition (16) as a random vector to account for uncertainties in the flight mode transitions. Furthermore, we assume that the probability density function (pdf) $p[\theta^*]$ is a multivariate Gaussian pdf with mean μ_θ and covariance Σ_θ; that is,

$$p[\theta^*] = \mathcal{N}_q(\theta^*; \mu_\theta, \Sigma_\theta) \tag{17}$$

Definition 1: The function $\mathcal{N}_q(y; \mu, \Sigma)$, denotes a q-dimensional multivariate Gaussian pdf with mean μ and covariance Σ. It is defined as

$$\mathcal{N}_q(y; \mu, \Sigma) := \frac{1}{(2\pi)^{\frac{q}{2}} |\Sigma|^{\frac{1}{2}}} \exp\left(-\frac{1}{2}(y-\mu)^T \Sigma^{-1} (y-\mu)\right) \tag{18}$$

where μ is a q-dimensional vector and Σ is a $q \times q$ symmetric positive-definite matrix. The mean μ_θ in Eq. (17) usually corresponds to the parameter that describes the nominal flight profile. Hence, μ_θ can be determined directly from a given flight plan or a standard terminal flight route, and the process could be easily automated. The covariance Σ_θ describes the random deviations of typical flight profiles from the nominal due to navigation uncertainties. For example, Σ_θ could be determined based on the required navigation performance for current operations or based on aircraft navigation performance for performance-based operations under NextGen. For best performance, it may be necessary to determine Σ_θ for various types of aircraft with different navigation performance levels, but it is not necessary to do this for every airport or every FCP. Our simulation results, given in Sec. IV, verify that the proposed tracking algorithm is not sensitive to variations in Σ_θ.

Because of the uncertainty of the aircraft flight profiles, as described previously, the flight mode transitions become probabilistic events. Let m_i and m_j be any two modes of the aircraft. We define the conditional (continuous-state-dependent) mode transition probability as

$$\pi_{ij}(x) := Pr[m_i \to m_j | x] = Pr[\mathcal{C}_{ij} | x] \tag{19}$$

where $m_i \to m_j$ denotes the event of a mode transition from m_i to m_j, and $\mathcal{C}_{ij}$ is the corresponding guard condition. It is obvious that the mode transition probability for $\mathcal{C}_{ij} = \oslash$ and $\mathcal{C}_{ij} = \mathcal{I}$ are 0 and 1, respectively. Thus, we shall only be concerned with the computation of the conditional mode transition probability for the guard condition of the type $C_{ij} = L_x x + L_\theta \theta^* \le 0$. We shall only consider absolutely continuous probability distributions. Hence, we consider the guard conditions $L_x x + L_\theta \theta^* \le 0$ and $L_x x + L_\theta \theta^* < 0$ to have

Table 5 Set of guard conditions for FCP_{10}

$$\begin{gathered}
\mathcal{C}_{11} = \mathcal{C}_{21} = \mathcal{C}_{31} = \neg\mathcal{C}_{12} \\
\mathcal{C}_{12} = \mathcal{C}_{22} = \mathcal{C}_{32} = L_x x + L_\theta \theta^* \le 0 \\
\mathcal{C}_{13} = \mathcal{C}_{23} = \mathcal{C}_{33} = \oslash \\
\mathcal{C}_{44} = \mathcal{C}_{54} = \oslash \\
\mathcal{C}_{45} = \mathcal{C}_{55} = \mathcal{I} \\
L_x = [\cos(\beta_1) \quad 0 \quad 0 \quad \sin(\beta_1) \quad 0 \quad 0 \quad 0 \quad 0] \\
L_\theta = -1 \\
\theta^* = d_1^* + \xi_{\text{ref}} \cos(\beta_1) + \eta_{\text{ref}} \sin(\beta_1)
\end{gathered}$$

Table 6 Set of guard conditions for FCP_{11}

$$\begin{gathered}
\mathcal{C}_{11} = \mathcal{C}_{21} = \mathcal{C}_{31} = L_x x + L_\theta \theta^* \le 0 \\
\mathcal{C}_{12} = \mathcal{C}_{22} = \mathcal{C}_{32} = \neg\mathcal{C}_{11} \\
\mathcal{C}_{13} = \mathcal{C}_{23} = \mathcal{C}_{33} = \oslash \\
\mathcal{C}_{44} = \mathcal{C}_{54} = \oslash \\
\mathcal{C}_{45} = \mathcal{C}_{55} = \mathcal{I} \\
L_x = [\cos(\beta_2) \quad 0 \quad 0 \quad -\sin(\beta_2) \quad 0 \quad 0 \quad 0 \quad 0] \\
L_\theta = 1 \\
\theta^* = d_2^* + \xi_{\text{ref}} \cos(\beta_2) + \eta_{\text{ref}} \sin(\beta_2)
\end{gathered}$$

the same probabilities. We define a multivariate Gaussian cdf $\Phi_q(\mu, \Sigma)$ as follows

Definition 2: Suppose $y = [y_1\ y_2\ \dots\ y_q]^T$ is a normal q-dimensional variate {i.e., $p[y] = \mathcal{N}_q(y; \mu, \Sigma)$}, then

$$\Phi_q(\mu, \Sigma) := Pr[y \le 0] = \int_{-\infty}^{0} \mathcal{N}_q(y; \mu, \Sigma)\mathrm{d}y = \int_{-\infty}^{-\mu} \mathcal{N}_q(y; 0, \Sigma)\mathrm{d}y \tag{20}$$

Note that we use the following notation for simplicity:

$$\int_{-\infty}^{a} \mathcal{N}_q(y; \mu, \Sigma)\mathrm{d}y := \int_{-\infty}^{a_1}\int_{-\infty}^{a_2}\dots\int_{-\infty}^{a_q} \mathcal{N}_q(y; \mu, \Sigma)\mathrm{d}y_1\mathrm{d}y_2\dots\mathrm{d}y_q \tag{21}$$

From Eq. (19), the conditional mode transition probability π_{ij} can be written as

$$\pi_{ij}(x) = Pr[L_x x + L_\theta \theta^* \le 0 | x] \tag{22}$$

From Eq. (17), we have

$$p[L_x x + L_\theta \theta^* | x] = \mathcal{N}_q(\theta^*; L_\theta \mu_\theta + L_x x, L_\theta \Sigma_\theta L_\theta^T) \tag{23}$$

Hence, from Eq. (23) and Definition 2, we have

$$\pi_{ij}(x) = \Phi_q(L_\theta \mu_\theta + L_x x, L_\theta \Sigma_\theta L_\theta^T) \tag{24}$$

D. General Stochastic Hybrid System Model

We now extend the aircraft dynamics model described in Secs. II.A–II.C to a general one consisting of r number of modes. The dynamics of the aircraft are described by

$$x(k+1) = A_{m(k)}x(k) + B_{m(k)}w_{m(k)}(k) \tag{25}$$

$$z(k) = C_{m(k)}x(k) + v_{m(k)}(k) \tag{26}$$

where $x(k) \in X = \mathbb{R}^n$ and $z(k) \in \mathbb{R}^p$ are the (discrete-time) continuous state and the measurement variables, respectively; $m(k) \in M = \{1, 2, \dots, r\}$ is the discrete state (or mode); and the process noise $w_{m(k)}(k)$ and the measurement noise $v_{m(k)}(k)$ are uncorrelated zero-mean Gaussian sequences. Let $\theta^* \in \Theta = \mathbb{R}^q$ be a random vector with pdf

$$p[\theta^*] = \mathcal{N}_q(\theta^*; \mu_\theta, \Sigma_\theta) \tag{27}$$

We define the vector space $\Omega = X \times \Theta$. For each mode transition from mode i to mode j, we define a guard condition $\mathcal{C}_{ij}$ as a polytopic subset (possibly empty) of Ω described by

$$L_{x,ij}x + L_{\theta,ij}\theta^* \le 0 \tag{28}$$

Furthermore, we assume that the set of guard conditions $\{\mathcal{C}_{ij} | j \in M\}$ forms an interiorly disjoint polytopic partition of the vector space Ω, as follows.

Assumption 1: For each $i \in M$, the intersection $\mathcal{C}_{ij} \cap \mathcal{C}_{il} = 0$ for all $j \ne l$.

Assumption 2: For each $i \in M$, the union $\cup_{j=1}^{r}\mathcal{C}_{ij} = \Omega$.

The evolution of mode $m(k)$ is then described by a continuous-state-dependent mode transition matrix:

$$\Pi(x(k)) = \{\pi_{ij}(x(k))\}_{i,j=1\dots r} \tag{29}$$

where

$$\pi_{ij}(x) := \Phi_q(L_{\theta,ij}\mu_\theta + L_{x,ij}x, L_{\theta,ij}\Sigma_\theta L_{\theta,ij}^T) \tag{30}$$

Assumptions 1 and 2 are needed to ensure that $\Pi(x(k))$ is a Markov transition matrix [23].

It can be verified that the aircraft dynamics model described in Secs. II.A–II.C is a special case of the hybrid system (25–30). For example, let us consider the submode transitions in the horizontal plane for FCP_2 (see Table 2). As illustrated in Fig. 10, the set of guard conditions $\{\mathcal{C}_{11}, \mathcal{C}_{12}, \mathcal{C}_{13}\}$ forms a polytopic partition of the vector space $\Omega = [\,h \quad h_2^*\,]$.

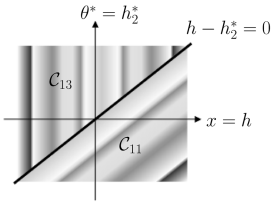

Fig. 10 Illustration of the polytopic partitioning of the vector space $\Omega = [\,h \quad h_2^*\,]$ by the set of guard conditions $\{\mathcal{C}_{11}, \mathcal{C}_{12}, \mathcal{C}_{13}\}$ for FTP_2. Note that $\mathcal{C}_{12}$ is empty.

III. Estimation Algorithm for Aircraft Tracking

A. Problem Formulation

Consider the general aircraft dynamic model [24–29]. Let $M^k = [m(1), m(2), \dots, m(k)]$ denote the mode history up to time k. Note that

$$m(1), m(2), \dots, m(k) \in \{1, 2, \dots, r\}$$

and thus the number of possible mode histories at time k is r^k. Let $Z^k = [z(1), z(2), \dots, z(k)]$ denote measurements up to time k. The aircraft-tracking problem involves estimating both the continuous-state pdf $p[x(k)|Z^k]$ and the mode pdf $p[m(k)|Z^k]$ from the measurements Z^k. By the total probability theorem, it can be shown that the pdf of the continuous state at any time k is given by

$$p[x(k)|Z^k] = \sum_{l=1}^{r^k} p[x(k)|Z^k, M_l^k]p[M^k = M_l^k|Z^k] \tag{31}$$

where M_l^k denotes the lth mode history. Hence, the computational complexity increases exponentially (as r^k). To overcome this problem, we use the Gaussian approximation method of the IMM algorithm [17]. The details of this method will be discussed in Sec. III.C.

A second problem arises due to the conditional mode transition probability $\pi_{ij}(x(k))$. The mode transition probability at time $k+1$ is updated by

$$p[m(k+1) = j|M^k, Z^k] = \int_{\mathbb{R}^n} p[m(k+1) = j|M^k, Z^k, x]p[x(k) = x|M^k, Z^k]\mathrm{d}x \tag{32}$$

We consider a continuous-state-dependent Markov mode transition, whereby the mode at time $k+1$ is dependent only on the mode and the continuous state at time k:

$$p[m(k+1) = j|M^k, Z^k, x(k)] = p[m(k+1) = j|m(k) = i, x(k)] = \pi_{ij}(x(k)) \tag{33}$$

Hence, using Eq. (32), Eq. (33) can be written as

$$p[m(k+1) = j|M^k, Z^k] = \int_{\mathbb{R}^n} \pi_{ij}(x)p[x(k) = x|M^k, Z^k]\mathrm{d}x \tag{34}$$

We denote $p[m(k+1) = j|M^k, Z^k]$ as the mode transition probability. Note that it is different from $\pi_{ij}(x)$ in that it is not conditioned on the continuous state.

Substituting Eq. (30) into Eq. (34), we have

$$p[m(k+1) = j|M^k, Z^k] = \int_{\mathbb{R}^n} \Phi_q(L_{x,ij}x + L_{\theta,ij}\mu_\theta, L_{\theta,ij}\Sigma_\theta L_{\theta,ij}^T)p[x(k) = x|M^k, Z^k]\mathrm{d}x \tag{35}$$

The multivariate integral (35) may be evaluated directly by numerical integration methods such as Gaussian quadratures or Monte Carlo integration methods. However, the computational cost of evaluating the integral would be very high if the dimension n is large. In the following section, we present an analysis that may greatly reduce the computational cost of evaluating the integral.

B. Algorithm for Computation of Mode Transition Probabilities

We first introduce the following Lemma, which will be used to compute the mode transition probability

$$p[m(k+1)=j|M^k, Z^k]$$

given in Eq. (35).

Lemma 1 Suppose that $y \in \mathbb{R}^n$ is a centered normal n-dimensional variate [i.e., $y \sim \mathcal{N}_n(y; 0, \Sigma_2)$], where $\Sigma_2 \in \mathbb{R}^{n\times n}$ is a symmetric positive-definite matrix. Let $a \in \mathbb{R}^q$ and $L \in \mathbb{R}^{q\times n}$, and let $\Sigma_1 \in \mathbb{R}^{q\times q}$ be a symmetric positive-definite matrix. Then the integral

$$\mathbb{J}_{mn} = \int_{\mathbb{R}^n} \Phi_q(a+Ly; \Sigma_1)\mathcal{N}_n(y; 0, \Sigma_2)\mathrm{d}y = \Phi_q(a; \tilde{\Sigma}) \tag{36}$$

where

$$\tilde{\Sigma} = \Sigma_1 + L\Sigma_2 L^T \tag{37}$$

Proof: By Definitions 1 and 2,

$$\begin{aligned}\mathbb{J}_{mn} &= \int_{\mathbb{R}^n}\int_{-\infty}^{-(a+Ly)} \mathcal{N}_q(\lambda; 0, \Sigma_1)\mathrm{d}\lambda\mathcal{N}_n(y; 0, \Sigma_2)\mathrm{d}y \\ &= \frac{1}{(2\pi)^{\frac{q+n}{2}}|\Sigma_1|^{\frac{1}{2}}|\Sigma_2|^{\frac{1}{2}}}\int_{\mathbb{R}^n}\int_{-\infty}^{-(a+Ly)} \\ &\quad\times \exp\left(-\frac{1}{2}[\lambda^T\Sigma_1^{-1}\lambda + y^T\Sigma_2^{-1}y]\right)\mathrm{d}\lambda\mathrm{d}y\end{aligned} \tag{38}$$

By substituting $\tilde{\lambda} = \lambda - Ly$ into Eq. (38) and by changing the order of integration,

$$\begin{aligned}\mathbb{J}_{mn} &= \frac{1}{(2\pi)^{\frac{q+n}{2}}|\Sigma_1|^{\frac{1}{2}}|\Sigma_2|^{\frac{1}{2}}}\int_{-\infty}^{-a}\int_{\mathbb{R}^n} \\ &\quad\times \exp\left(-\frac{1}{2}[(\tilde{\lambda}+Ly)^T\Sigma_1^{-1}(\tilde{\lambda}+Ly) + y^T\Sigma_2^{-1}y]\right)\mathrm{d}y\mathrm{d}\tilde{\lambda}\end{aligned} \tag{39}$$

We can verify that

$$\begin{aligned}&(\tilde{\lambda}+Ly)^T\Sigma_1^{-1}(\tilde{\lambda}+Ly) + y^T\Sigma_2^{-1}y \\ &\quad= [y + (\Sigma_2^{-1} + L^T\Sigma_1^{-1}L)^{-1}L^T\Sigma_1^{-1}\tilde{\lambda}]^T(\Sigma_2^{-1} + L^T\Sigma_1^{-1}L) \\ &\quad\times [y + (\Sigma_2^{-1} + L^T\Sigma_1^{-1}L)^{-1}L^T\Sigma_1^{-1}\tilde{\lambda}] \\ &\quad+ \tilde{\lambda}^T[\Sigma_1^{-1} - \Sigma_1^{-1}L(\Sigma_2^{-1} + L^T\Sigma_1^{-1}L)^{-1}L^T\Sigma_1^{-1}]\tilde{\lambda}\end{aligned} \tag{40}$$

Substituting Eq. (40) into the exponential term in Eq. (39), we have

$$\begin{aligned}\mathbb{J}_{mn} &= \frac{1}{(2\pi)^{\frac{q}{2}}|\Sigma_1|^{\frac{1}{2}}|\Sigma_2|^{\frac{1}{2}}|\Sigma_2^{-1} + L^T\Sigma_1^{-1}L|^{\frac{1}{2}}}\int_{-\infty}^{-a} \\ &\quad\times \exp\left(-\frac{1}{2}\tilde{\lambda}^T[\Sigma_1^{-1} - \Sigma_1^{-1}L(\Sigma_2^{-1} + L^T\Sigma_1^{-1}L)^{-1}L^T\Sigma_1^{-1}]\tilde{\lambda}\right)\mathrm{d}\tilde{\lambda}\end{aligned} \tag{41}$$

Using the matrix inversion lemma [24], we have

$$\begin{aligned}&\Sigma_1^{-1} - \Sigma_1^{-1}L(\Sigma_2^{-1} + L^T\Sigma_1^{-1}L)^{-1}L^T\Sigma_1^{-1} \\ &\quad= (\Sigma_1 + L\Sigma_2L^T)^{-1} = \tilde{\Sigma}^{-1}\end{aligned} \tag{42}$$

$$|\Sigma_1||\Sigma_2||\Sigma_2^{-1} + L^T\Sigma_1^{-1}L| = |\Sigma_1 + L\Sigma_2L^T| = |\tilde{\Sigma}| \tag{43}$$

Hence,

$$\mathbb{J}_{mn} = \frac{1}{(2\pi)^{\frac{q}{2}}|\tilde{\Sigma}|^{\frac{1}{2}}}\int_{-\infty}^{-a}\exp\left(-\frac{1}{2}\tilde{\lambda}^T\tilde{\Sigma}^{-1}\tilde{\lambda}\right)\mathrm{d}\tilde{\lambda} = \Phi_q(a, \tilde{\Sigma}) \tag{44}$$

The following assumption is used in the computation of the mode transition probability:

$$p[m(k+1)=j|M^k, Z^k]$$

We will see later that this assumption is also needed to overcome the problem of exponentially growing complexity.

Assumption 3: Gaussian Approximation. The pdf of the state at time k is conditioned on the past measurements Z^k and the mode history M^k is given by

$$\begin{aligned}&p[x(k)=x|M^k, Z^k] = p[x(k)=x|m(k)=i, Z^k] \\ &r = \mathcal{N}_n(x; \hat{x}_i(k), P_i(k)) \qquad i=1,2,\ldots,r\end{aligned} \tag{45}$$

In other words, we assume that the state pdf at time k is a Gaussian pdf with mean $\hat{x}_i(k)$ and covariance $P_i(k)$ that depends on the mode at time k. We now present the Lemma that is used to evaluate the mode transition probability given in Eq. (35).

Lemma 2 Under Assumption 3, the mode transition probability given in Eq. (37) can be evaluated as

$$\begin{aligned}&p[m(k+1)=j|M^k, Z^k] = p[m(k+1)=j|m(k)=i, Z^k] \\ &\quad= \Phi_q\left(L_{x,ij}\hat{x}_i(k) + L_{\theta,ij}\mu_\theta, L_{x,ij}P_i(k)L_{x,ij}^T + L_{\theta,ij}\Sigma_\theta L_{\theta,ij}^T\right)\end{aligned} \tag{46}$$

Proof: Under Assumption 3, the mode transition probability would be conditioned only in mode $m(k)=i$ instead of all the past mode history M^k. Substituting Eq. (45) of Assumption 3 into Eq. (35), we have

$$\begin{aligned}&p[m(k+1)=j|M^k, Z^k] = p[m(k+1)=j|m(k)=i, Z^k] \\ &\quad= \int_{\mathbb{R}^n}\Phi_q(L_{x,ij}x + L_{\theta,ij}\mu_\theta, L_{\theta,ij}\Sigma L_{\theta,ij}^T)\mathcal{N}(x; \hat{x}_i(k), P_i(k))\mathrm{d}x\end{aligned} \tag{47}$$

Substituting $x = \tilde{x} + \hat{x}_i$, we have

$$\begin{aligned}&p[m(k+1)=j|M^k, Z^k] = \int_{\mathbb{R}^n}\Phi_q(L_{ij}\tilde{x} + L_{ij}\hat{x}_i(k) \\ &\quad+ L_{\theta,ij}\mu_\theta, L_{\theta,ij}\Sigma L_{\theta,ij}^T)\mathcal{N}_n(\tilde{x}; 0, P_i(k))\mathrm{d}\tilde{x}\end{aligned} \tag{48}$$

The proof is then completed using Lemma 1.

Lemma 2 shows that the mode transition probability can be expressed in terms of the multivariate Gaussian cdf $\Phi_q(\cdot)$. As a result, the dimension of the integral (35) is reduced from $q+n$ to q. This result is especially useful if $q < n$, which is the case in our application. For example, in all the mode transition models discussed in Sec. II, q is either 1 or 2 and the dimension of the continuous-state space n is 8. Using the method proposed by Genz [25] to compute the Gaussian cdf, the computational cost could be reduced from about 2 s when the dimension of the cdf is 10 to about 0.1 s when the dimension is 3.

Further usefulness of the lemma is that although the multivariate Gaussian cdf does not have any closed-form formula in general, there are a number of algorithms that numerically estimate its values [25–29]. Furthermore, our algorithm is not sensitive to the accuracy of the estimated value for Eq. (46). An accuracy of 2 digits (0.01) would usually be sufficient. For $q=1$, the Gaussian cdf is well tabulated. For $q=2$ or 3, closed-form formulas given by Cox and Wermuth [26], which provide sufficiently good estimations, may be used. For general cases in which $q \geq 4$, various efficient numerical estimations based on Monte Carlo procedures combined with analytical methods have been proposed by Genz [25] and Deak [27]. The algorithm proposed by Deak [27], for example, yields 3-digit accuracy, in the worst case, in less than 1 s for all dimensions $q \leq 20$. For moderate dimensions $q \leq 7$, an algorithm based on recursive

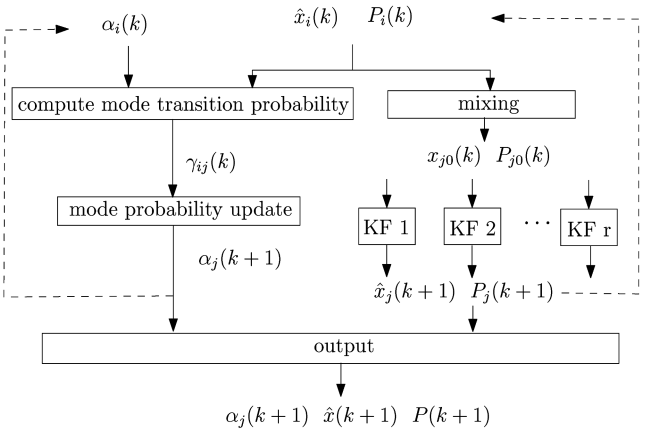

Fig. 11 Structure of the hybrid estimation algorithm.

integration, proposed by Miwa et al. [28], has been shown to be faster than that based on Monte Carlo procedure. The reader may also refer to Tong [29] for discussions of other numerical algorithms.

C. Hybrid Estimation Algorithm

As shown in Fig. 11, the hybrid estimation algorithm consists of a bank of r mode-matched Kalman filters (KF) that run recursively. Assume that at time k, we have the posterior mode probability (or the discrete-state pdf) $\alpha_i(k|k)$, which is defined as

$$\alpha_i(k|k) := p[m(k) = i|Z^k] \quad \text{for } i = 1, \ldots, r \tag{49}$$

We also have a posterior continuous-state pdf from each Kalman filter i, given by

$$p[x(k) = x|m(k) = i, Z^k] = \mathcal{N}_n(x; \hat{x}_i(k|k), P_i(k|k)) \tag{50}$$

where $\hat{x}_i(k|k)$ and $P_i(k|k)$ are the posterior mean and covariance matrix, respectively, from Kalman filter i. The continuous-state pdf and the discrete-state pdf at time $k+1$ are then updated as follows.

1. *Compute Mode Transition Probability*

As shown in Lemma 2, the mode transition probability given in Eq. (34) can be written as

$$p[m(k+1) = j|M^k, Z^k] = p[m(k+1) = j|m(k) = i, Z^k] \tag{51}$$

Thus, from here on, we denote the mode transition probability as $\gamma_{ij}(k)$:

$$\begin{aligned}\gamma_{ij}(k) &:= p[m(k+1) = j|m(k) = i, Z^k] \\ &= \Phi_q(L_{x,ij}\hat{x}_i(k) + L_{\theta,ij}\mu_\theta, L_{x,ij}P_i(k)L_{x,ij}^T + L_{\theta,ij}\Sigma_\theta L_{\theta,ij}^T)\end{aligned} \tag{52}$$

2. *Mixing*

As discussed in Sec. III.A, the computational complexity grows exponentially if we consider all past mode histories when updating the continuous-state pdf. We use the Gaussian approximation method in the IMM algorithm [17] to overcome this problem. From r Kalman filters, we have

$$\begin{aligned}p[x(k+1)|Z^{k+1}] &= \sum_{j=1}^{r} p[x(k+1)|m(k+1) \\ &\quad = j, Z^{k+1}]p[m(k+1) = j|Z^{k+1}]\end{aligned} \tag{53}$$

where

$$\begin{aligned}&p[x(k+1)|m(k+1) = j, Z^{k+1}] \\ &\quad = \frac{p[z(k+1)|x(k+1), m(k+1) = j, Z^k]}{p[z(k+1)|m(k+1) = j, Z^k]} \\ &\quad \times p[x(k+1)|m(k+1) = j, Z^k]\end{aligned} \tag{54}$$

The last term on the right of Eq. (54) can be written as

$$\begin{aligned}p[x(k+1)|m(k+1) = j, Z^k] &= \sum_{i=1}^{r} p[x(k+1)|m(k+1) \\ &\quad = j, m(k) = i, Z^k]p[m(k) = i|m(k+1) = j, Z^k]\end{aligned} \tag{55}$$

Assumption 4: Gaussian Approximation. Similar to Assumption 3, we assume that each of the pdf

$$p[x(k+1)|m(k+1) = j, m(k) = i, Z^k]$$

is Gaussian and is conditioned only on the mean and covariance of Kalman filter i computed at time k. In other words,

$$\begin{aligned}&p[x(k+1)|m(k+1) = j, m(k) = i, Z^k] \\ &\quad = p[x(k+1)|m(k+1) = j, \hat{x}_i(k), P_i(k)]\end{aligned} \tag{56}$$

is a Gaussian pdf with a mean and covariance that depend on $\hat{x}_i(k)$ and $P_i(k)$. The pdf

$$p[x(k+1)|m(k+1) = j, Z^k]$$

in Eq. (55) is then approximated via moment matching by a single Gaussian pdf. Hence, we compute the initial conditions $\hat{x}_{j0}(k)$ and $P_{j0}(k)$, which are the inputs to each Kalman filter j, as follows:

$$\hat{x}_{j0}(k) = \sum_{i=1}^{r} \hat{x}_i(k|k)\bar{\alpha}_{ji}(k) \tag{57}$$

$$P_{j0}(k) = \sum_{i=1}^{r} \{P_i(k|k) + [\hat{x}_i(k|k) - \hat{x}_{j0}(k)][\hat{x}_i(k|k) - \hat{x}_{j0}(k)]^T\}\bar{\alpha}_{ji}(k) \tag{58}$$

where

$$\bar{\alpha}_{ji}(k) := p[m(k) = i|m(k+1) = j, Z^k] = \frac{1}{c_j}\gamma_{ij}(k)\alpha_i(k|k) \tag{59}$$

and c_j is a normalizing constant.

3. *Filtering*

Each Kalman filter j computes its own posteriors $\hat{x}_j(k+1|k+1)$ and $P_j(k+1|k+1)$ using the initial conditions $\hat{x}_{j0}(k)$ and $P_{j0}(k)$.

4. *Mode Probability Update*

For $j = 1, \ldots, r$, the prior probability of mode j is given by

$$\alpha_j(k+1|k) := p[m(k+1) = j|Z^k] = \sum_{i=1}^{r} \gamma_{ij}(k)\alpha_i(k|k) \tag{60}$$

Next, define the likelihood function for Kalman filter j:

$$\begin{aligned}\Lambda_j(k+1) &:= p[z(k+1)|m(k+1) = j, Z^k] \\ &= \mathcal{N}_p(r_j(k+1); 0, S_j(k+1))\end{aligned} \tag{61}$$

where

$$r_j(k+1) = z(k+1) - C_j\hat{x}_j(k+1|k+1)$$

is the residual of Kalman filter j, and $S_j(k+1)$ is its covariance. The posterior probability of mode j is then given by

$$\alpha_j(k+1|k+1) = \tfrac{1}{\beta} p[z(k+1)|m(k+1)=j, Z^k] p[m(k+1) = j|Z^k] = \tfrac{1}{\beta}\Lambda_j(k)\alpha_j(k+1|k) \quad (62)$$

where β is a normalizing constant.

5. Output

The continuous-state pdf at time $k+1$ is given by

$$p[x(k+1)=x|Z^{k+1}] = \sum_{j=1}^{r} \mathcal{N}_n(x; \hat{x}_j(k+1|k+1), P_j(k+1|k+1))\alpha_j(k+1|k+1) \approx \mathcal{N}_n(x; \hat{x}(k+1), P(k+1)) \quad (63)$$

where

$$\hat{x}(k+1) = \sum_{j=1}^{r} \hat{x}_j(k+1|k+1)\alpha_j(k+1|k+1) \quad (64)$$

$$P(k+1) = \sum_{j=1}^{r} \{P_j(k+1|k+1) + [\hat{x}_j(k+1|k+1) - \hat{x}(k)] \cdot [\hat{x}_j(k+1|k+1) - \hat{x}(k)]^T\}\alpha_j(k+1|k+1) \quad (65)$$

The discrete-state pdf at time $k+1$ is given by

$$p[m(k+1)=j|Z^{k+1}] = \alpha_j(k+1|k+1) \quad \text{for } j = 1, \ldots, r \quad (66)$$

IV. Simulations

We illustrate the application of our algorithm to two aircraft-tracking scenarios. For ease of presentation, we would like to reduce the number of flight modes to be considered in each scenario. Hence, for the first scenario, which involves an aircraft flying at constant altitude along a STAR, we consider only the horizontal submodes. For the second scenario, which involves a landing aircraft, we consider only the vertical submodes.

A. Example 1: Aircraft Movement Along STAR

1. Simulation Scenario

We consider an aircraft arriving along a STAR, similar to the example given in Sec. II.A (Fig. 8). To emulate actual arrival aircraft trajectories [11], we generated 60 aircraft trajectories that are randomly distributed about the nominal trajectory, as shown in Fig. 12. The nominal speed of the aircraft is 500 kt and its nominal turning rate during a coordinated turn is 1.5 deg/s.

We denote the algorithm proposed in Sec. III.C as the state-dependent-transition hybrid estimation (SDTHE) algorithm. We compare the performance of the SDTHE algorithm with that of the IMM algorithm, which has been shown to have great performance in aircraft-tracking applications in terms of tracking accuracy and computation time [11,14]. The IMM algorithm models the mode transition using a constant matrix Π that is independent of the continuous state. For this simulation, for simplicity, we assume that the aircraft is always flying at constant altitude, and hence the aircraft submode in the vertical plane is always CH. Thus, we consider only the submodes in the horizontal plane. We consider two designs of the mode transition matrix for the IMM algorithm:

$$\text{IMM 1:}\Pi = \begin{bmatrix} \pi_{11} & \pi_{12} & \pi_{13} \\ \pi_{21} & \pi_{22} & \pi_{23} \\ \pi_{31} & \pi_{32} & \pi_{33} \end{bmatrix} = \begin{bmatrix} 0.8 & 0.1 & 0.1 \\ 0.1 & 0.8 & 0.1 \\ 0.1 & 0.1 & 0.8 \end{bmatrix}$$

$$\text{IMM2:}\Pi = \begin{bmatrix} 0.95 & 0.025 & 0.025 \\ 0.025 & 0.95 & 0.025 \\ 0.025 & 0.025 & 0.95 \end{bmatrix}$$

Thus, in the IMM algorithm, the mode transition probabilities π_{ij} are all constant. Higher values in the offdiagonal terms of the mode transition matrix Π correspond to higher probabilities of mode transitions. Hence, the first design (IMM1) assumes a higher probability of mode transitions compared with the second design (IMM2). We use these two designs to investigate the effect of the mode transition probability matrix on its tracking performance. For the SDTHE algorithm, we model the mode transitions of FCP_{10} as given in Table 3. Hence,

$$\pi_{11} = \pi_{21} = \pi_{31} = 1 - p[d_{s1} \le d_1^*|x] = 1 - \Phi_1(L_1 x - \bar{d}_1^*; \Sigma_{d_1^*}) \quad (67)$$

$$\pi_{12} = \pi_{22} = \pi_{32} = p[d_{s1} \le d_1^*|x] = \Phi_1(L_1 x - \bar{d}_1^*; \Sigma_{d_1^*}) \quad (68)$$

$$\pi_{13} = \pi_{23} = \pi_{33} = 0 \quad (69)$$

where

$$L_1 = [\cos(\beta_1) \quad 0 \quad 0 \quad \sin(\beta_1) \quad 0 \quad 0 \quad 0 \quad 0]$$

To account for exceptional flight scenarios, such as a collision-avoidance maneuver, we include a small constant term (0.01) in each π_{ij}. This term is added so that there is always a small probability ($\approx$0.01) of an aircraft mode change regardless of the continuous state of the aircraft. Thus, we use the following modified conditional mode transition probabilities:

$$\pi_{11} = \pi_{21} = \pi_{31} = \kappa(\Phi_1(L_1 x - \bar{d}_1^*; \Sigma_{d_1^*}) + 0.01) \quad (70)$$

$$\pi_{12} = \pi_{22} = \pi_{32} = \kappa(1.01 - \Phi_1(L_1 x - \bar{d}_1^*; \Sigma_{d_1^*})) \quad (71)$$

$$\pi_{13} = \pi_{23} = \pi_{33} = 0.01\kappa \quad (72)$$

The constant $\kappa = 1/1.03$ is used as a normalizing factor, so that

$$\sum_{j=1}^{r} \pi_{ij} = 1$$

for all $i = 1, 2, 3$. The parameter d_1^* depends on the point (corresponds to FCP_{10} in Fig. 8) at which the aircraft starts to turn. It is assumed to have a distribution

$$p[d_1^*] = \mathcal{N}_1(d_1^*; \bar{d}_1^*, \Sigma_{d_1^*})$$

where the mean distance $\bar{d}_1^*$ is given in Fig. 12, and the covariance $\Sigma_{d_1^*}$ is $(0.5\ \text{nm})^2$. Similarly, the conditional mode transition probabilities for FCP_{11} are given by

$$\pi_{11} = \pi_{21} = \pi_{31} = \kappa(\Phi_1(L_2 x - \bar{d}_2^*; \Sigma_{d_2^*}) + 0.01) \quad (73)$$

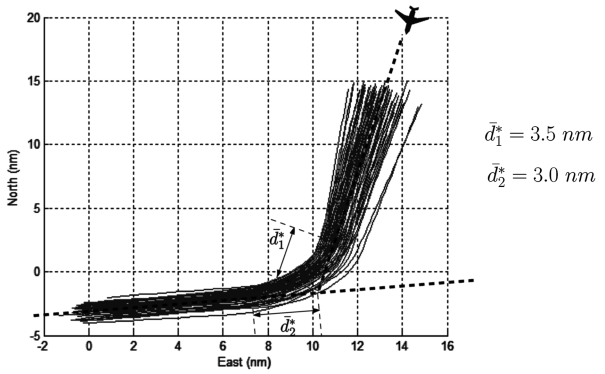

Fig. 12 Sixty simulated trajectories for arrival aircraft for which the flight plans filed the STAR given in Fig. 8.

$$\pi_{12} = \pi_{22} = \pi_{32} = \kappa(1.01 - \Phi_1(L_2 x - \bar{d}_2^*; \Sigma_{d_2^*})) \quad (74)$$

$$\pi_{13} = \pi_{23} = \pi_{33} = 0.01\kappa \quad (75)$$

where

$$L_1 = [\cos(\beta_2) \quad 0 \quad 0 \quad \sin(\beta_2) \quad 0 \quad 0 \quad 0 \quad 0]$$

$\bar{d}_2^*$ is given in Fig. 12, and $\Sigma_{d_2^*}$ is $(0.5 \text{ nm})^2$.

2. Simulation Results

Figures 13 and 14 compare the tracking accuracy and the mode-estimation accuracy of the algorithms. The statistics of the results are summarized in Table 7. Note that the aircraft performs a coordinated turn at a time approximately between 50 and 100 s. From Fig. 13 and Table 7, the tracking accuracy of the IMM algorithm depends on the design of the mode transition matrix. The first design IMM1, which assumes high mode transition probabilities, does not have good tracking performance during steady-state motion, compared with both IMM2 and SDTHE. On the other hand, IMM2, which assumes low mode transition probabilities, has poor tracking performance at the onset of mode transitions. Furthermore, from Fig. 14 and Table 7, IMM2 performs badly in mode estimation. The SDTHE algorithm has both better tracking accuracy and better mode-estimation accuracy than both IMM1 and IMM2. In summary, the result shows that the IMM algorithm requires a tradeoff between peak estimation errors at the onset of mode transitions and average estimation errors during steady-state motions. The SDTHE algorithm is able to achieve better performance by conditioning the mode transition probabilities on the continuous state of the aircraft.

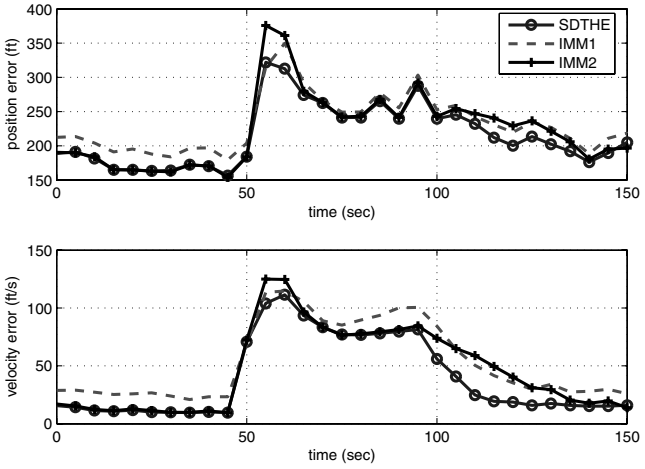

Fig. 13 Comparison of tracking accuracy for Example 1: rms values of position error for 60 runs.

B. Aircraft Landing

1. Simulation Scenario

We consider a typical aircraft landing profile similar to that given in the example discussed in Sec. II.B (Fig. 6). We simulate the descent phase from an altitude of about 22,000 ft down to about 10,000 ft. We generate 100 random descent profiles, as shown in Fig. 15 for the simulation. As before, we assume that a surveillance radar provides position measurements with a standard deviation of 300 ft in each axis of the local navigation frame at 5 s intervals.

For simplicity of illustration, we consider only the vertical-plane dynamics and hence only the CH and CD submodes. Again, we consider two designs for the IMM algorithm:

$$\text{IMM 1:}\Pi = \begin{bmatrix} \pi_{44} & \pi_{45} \\ \pi_{54} & \pi_{55} \end{bmatrix} = \begin{bmatrix} 0.8 & 0.2 \\ 0.2 & 0.8 \end{bmatrix}$$

$$\text{IMM2:}\Pi = \begin{bmatrix} 0.95 & 0.05 \\ 0.05 & 0.95 \end{bmatrix}$$

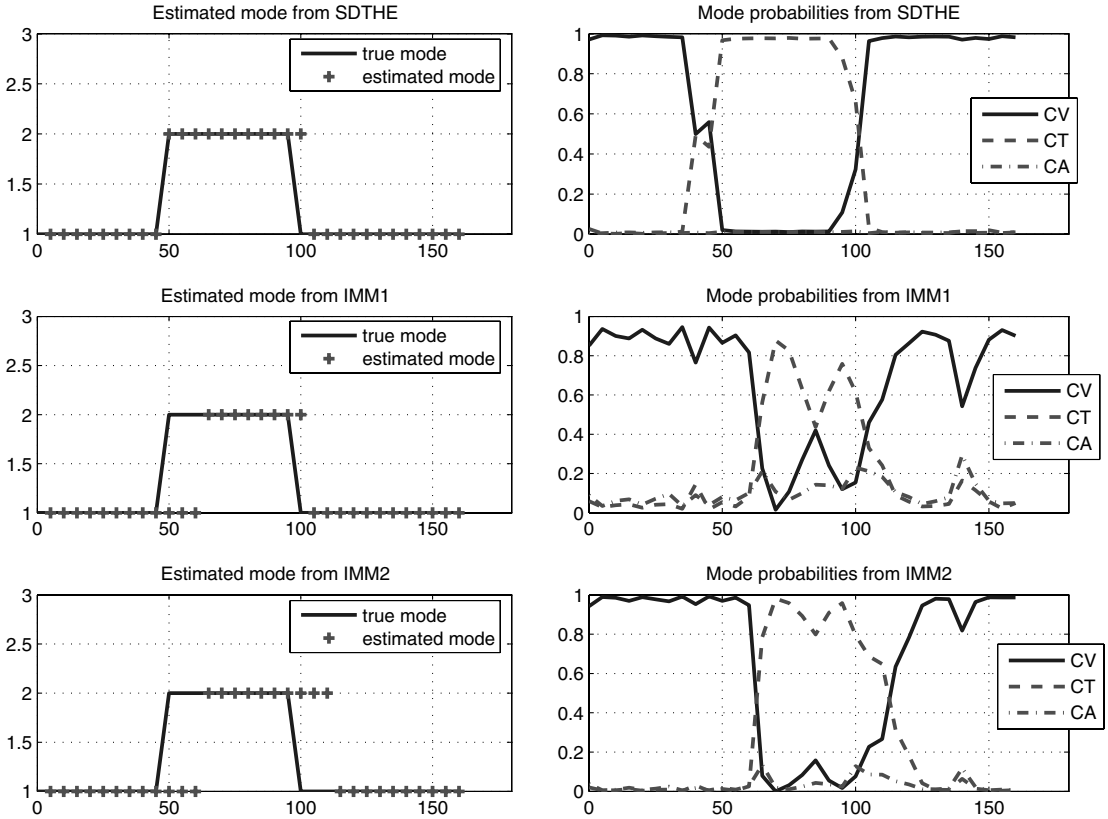

Fig. 14 Comparison of mode-estimation accuracy for Example 1: mode estimation and mode probabilities of a typical run.

Table 7 Comparison of performance for Example 1: statistics of 60 simulation runs

	RMS position error, ft		RMS velocity error, ft/s		Average mode-estimation error
	Peak	Average	Peak	Average	(number of time steps)
IMM1	350	228	115	49	5.8
IMM2	376	219	125	42	8.1
SDTHE	322	212	112	36	3.7

For the SDTHE algorithm, we use the mode transition models given in Tables 3 and 4. Thus, the conditional mode transition probabilities for FCP_3 are

$$\pi_{44} = \pi_{54} = \kappa(1.01 - \Phi_2(L_3 x - \mu_1; \Sigma_1)) \tag{76}$$

$$\pi_{45} = \pi_{55} = \kappa(\Phi_2(L_3 x - \mu_1; \Sigma_1) + 0.01) \tag{77}$$

where

$$L_3 = \begin{bmatrix} \cos(\psi) & 0 & 0 & \sin(\psi) & 0 & 0 & 0 & 0 \\ 0 & 0 & 0 & 0 & 0 & 0 & 1 & 0 \end{bmatrix}$$

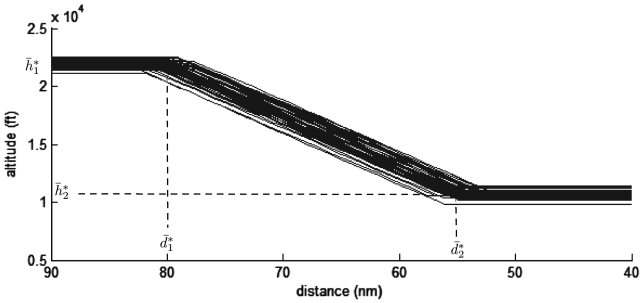

Fig. 15 One hundred simulated trajectories for a descent phase.

$$\mu_1 = \begin{bmatrix} \bar{d}_1^* \\ \bar{h}_1^* \end{bmatrix} = \begin{bmatrix} 80 \text{ nm} \\ 2100 \text{ ft} \end{bmatrix}$$

To investigate the sensitivity of the SDTHE algorithm to the assumed distribution of the parameters d_1^* and h_1^*, we consider two designs of

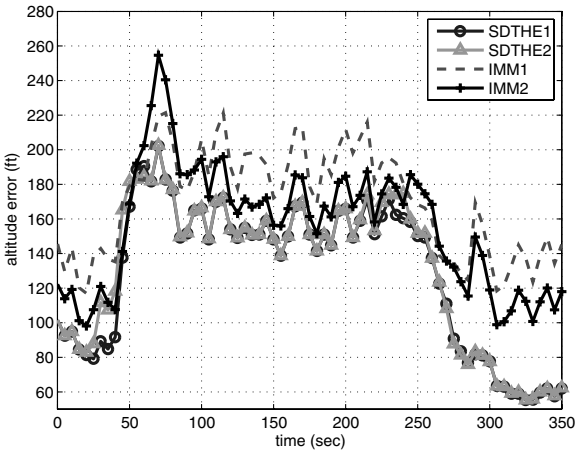

Fig. 16 Comparison of tracking accuracy for Example 2: rms values of altitude error for 100 runs.

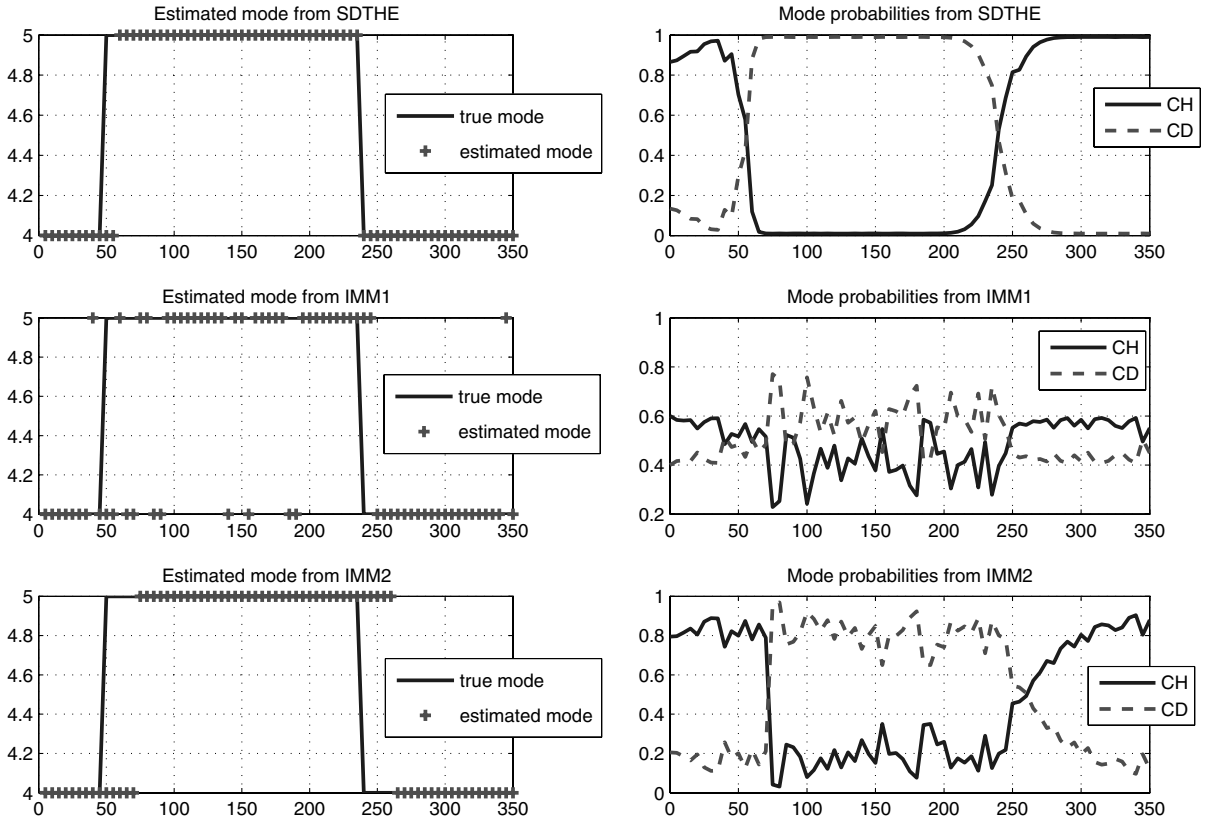

Fig. 17 Comparison of mode-estimation accuracy for Example 2: mode estimation and mode probabilities of a typical run.

the SDTHE algorithm. In the first design (SDTHE1), we use

$$\Sigma_1 = \begin{bmatrix} (1.5\text{ nm})^2 & 0 \\ 0 & (300\text{ ft})^2 \end{bmatrix}$$

which is close to the actual variations of the simulated trajectories. In the second design (SDTHE2), we use

$$\Sigma_1 = \begin{bmatrix} (3\text{ nm})^2 & 0 \\ 0 & (500\text{ ft})^2 \end{bmatrix}$$

.

The conditional mode transition probabilities for FCP_4 are

$$\pi_{44} = \pi_{45} = \kappa(1.01 - \Phi_2(L_4 x - \mu_2; \Sigma_2)) \tag{78}$$

$$\pi_{54} = \pi_{55} = \kappa(\Phi_2(L_4 x - \mu_2; \Sigma_2) + 0.01) \tag{79}$$

where

$$L_4 = \begin{bmatrix} \cos(\psi) & 0 & 0 & \sin(\psi) & 0 & 0 & 0 & 0 \\ 0 & 0 & 0 & 0 & 0 & 0 & 1 & 0 \end{bmatrix}$$

$$\mu_2 = \begin{bmatrix} \bar{d}_2^* \\ \bar{h}_2^* \end{bmatrix} = \begin{bmatrix} 55\text{ nm} \\ 10,500\text{ ft} \end{bmatrix}$$

$$\Sigma_2 = \Sigma_1$$

2. Simulation Results

Figures 16 and 17 compare the tracking accuracy and mode-estimation accuracy of the various algorithms. Here, we see that IMM1, which assumes high mode transition probabilities, has a number of errors in its mode-estimation, even during steady-state motion. The confidence level of the mode estimation, as measured by the mode probabilities, is also not good. On the other hand, IMM2, which assumes low mode transition probabilities, has large delays in detecting mode transitions. The SDTHE algorithm has better tracking accuracy and mode-estimation accuracy than both IMM1 and IMM2. Furthermore, the results of SDTHE1 and SDTHE2 show that the SDTHE algorithm is not sensitive to variations in the covariance of the parameters d_1^*, h_1^*, etc. The results of the 100 simulation runs are summarized in Table 8.

Table 9 shows the total run time for the 100 runs in both Example 1 and Example 2 for the various algorithms. The run time of the SDTHE algorithm is of the same order as that of IMM1 or IMM2.

Table 8 Comparison of performance for Example 2: statistics of 100 simulation runs

	RMS altitude error, ft		Average mode-estimation error
	Peak	Average	(number of time steps)
IMM1	221	171	11.7
IMM2	255	158	9.6
SDTHE1	202	133	2.8
SDTHE2	203	135	3.7

Table 9 Comparison of the respective total run time in Example 1 and Example 2

	Example 1 (60 runs)	Example 2 (100 runs)
IMM	3.4 s	6.0 s
SDTHE	3.6 s	7.2 s

V. Conclusions

We have proposed a stochastic linear system hybrid estimation algorithm for the tracking of aircraft around airports. In the algorithm, a methodology to model an aircraft's flight mode transitions based on its nominal flight profiles is proposed. An analytical result to reduce the computational cost of evaluating the mode transition probabilities is also presented. The performance of the algorithm has been illustrated with simulation examples.

We are currently investigating the application of the proposed aircraft model and estimation algorithm to aircraft conformance monitoring for future air traffic management operations, such as airborne spacing and sequencing operations, in the Next Generation Air Transportation System.

Acknowledgments

The authors would like to acknowledge that this work is supported by the National Science Foundation CAREER award CNS-0746299 and to thank Helen Gill for her support.

References

[1] Krishnamurthy, K., Barmore, B., Bussink, F., Weitz, L., and Dahlene, L., "Fast-Time Evaluations of Airborne Merging and Spacing in Terminal Arrival Operations," AIAA Guidance, Navigation, and Control Conference, AIAA Paper 2005-6143, Aug. 2005.

[2] *Introduction to TCAS II Version 7*, U.S. Dept. of Transportation, Federal Aviation Administration, Nov. 2000.

[3] Nivert, L. J., Walsh, J. A., and Wojciech, J. J., "Development of the Traffic Alert and Collision Avoidance System III (TCAS III)," *AIAA/IEEE Digital Avionics Systems Conference*, Pt. 2, AIAA, Reston, VA, 1988, pp. 871–876; also AIAA Paper 1988-4002.

[4] Erzerberger, H., and Tobias, L., "A Time-Based Concept for Terminal-Area Traffic Management," *Efficient Conduct of Individual Flights and Air Traffic*, AGARD, Neuilly-sur-Seine, France, 1986, pp. 63–84.

[5] Kuchar, J. K., and Yang, L. C., "A Review of Conflict Detection and Resolution Modeling Methods," *IEEE Transactions on Intelligent Transportation Systems*, Vol. 1, No. 4, 2000, pp. 179–189. doi:10.1109/6979.898217

[6] Naseri, A., and Neogi, N., "Stochastic Hybrid Models with Applications to Air Traffic Management," AIAA Guidance, Navigation, and Control Conference, Hilton Head, SC, AIAA Paper 2007-6696, 2007.

[7] Hwang, I., Hwang, J., and Tomlin, C., "Flight-Mode-Based Aircraft Conflict Detection Using a Residual—Mean Interacting Multiple Model Algorithm," AIAA Guidance, Navigation, and Control Conference, Austin, TX, AIAA Paper 2003-5340, Aug. 2003.

[8] Yepes, J. L., Hwang, I., and Rotea, M., "An Intent Based Trajectory Prediction Algorithm for Air Traffic Control," AIAA Guidance, Navigation, and Control Conference, San Francisco, AIAA Paper 2005-5824, Aug. 2005.

[9] Krozel, J., "Intent Inference for Free Flight Aircraft," AIAA Guidance, Navigation, and Control Conference, Denver, CO, AIAA Paper 2000-4479, Aug. 2000.

[10] Lymperopoulos, I., Lygeros, J., and Lecchini, A., "Model Based Aircraft Trajectory Prediction During Takeoff," AIAA Guidance, Navigation, and Control Conference, Keystone, CO, AIAA Paper 2006-6098, Aug. 2006.

[11] Roy, K., Levyy, B., and Tomlin, C., "Target Tracking and Estimated Time of Arrival (ETA) Prediction for Arrival Aircraft," *AIAA Guidance, Navigation, and Control Conference*, Keystone, CO, Aug. 2006.

[12] Anon., "Next Generation Air Transportation System (NextGen) Information Paper," Tenth Meeting of Civil Aviation Authorities, Caracas, Venezuela, Paper International Civil Aviation Organization Paper RAAC/10-IP/03, June 2007.

[13] Bar-Shalom, Y., Rong Li, X., and Kirubarajan, T., *Estimation with Applications to Tracking and Navigation*, 1st ed., Wiley, Hoboken, NJ, 2001, pp. 421–490.

[14] Li, X. R., and Bar-Shalom, Y., "Design of an Interacting Multiple Model Algorithm for Air Traffic Control Tracking," *IEEE Transactions on Control Systems Technology*, Vol. 1, No. 3, 1993, pp. 186–194. doi:10.1109/87.251886

[15] Hwang, I., Balakrishnan, H., and Tomlin, C., "State Estimation for Hybrid Systems: Applications to Aircraft Tracking," *IEE Proceedings: Control, Theory and Applications*, Vol. 153, No. 5, Sept. 2006, pp. 556–566. doi:10.1049/ip-cta:20050053

[16] Nolan, M. S., *Fundamentals of Air Traffic Control*, Brooks/Cole, Albany, NY, 1998, pp. 136–141.
[17] Blom, H. A. P., and Bar-Shalom, Y., "The Interacting Multiple Model Algorithm for Systems with Markovian Switching Coefficients," *IEEE Transactions on Automatic Control*, Vol. 33, No. 8, 1988, pp. 780–783. doi:10.1109/9.1299
[18] Doucet, A., Gordon, N., and Krishnamurthy, V., "Particle Filters for State Estimation of Jump Markov Linear Systems," *IEEE Transactions on Signal Processing*, Vol. 49, No. 3, Mar. 2001, pp. 613–624. doi:10.1109/78.905890
[19] Blom, H. A. P., and Bloem, E. A., "Particle Filtering for Stochastic Hybrid Systems," *Proceedings of the 43rd IEEE Conference on Decision and Control, Atlantis*, Inst. of Electrical and Electronics Engineers, Piscataway, NJ, 2004, pp. 3221–3226.
[20] Seah, C. E., and Hwang, I., "Hybrid Estimation Algorithm Using State-Dependent Mode Transition Matrix for Aircraft Tracking," AIAA Guidance, Navigation, and Control Conference, Keystone, CO, AIAA Paper 2006-6245, Aug. 2006.
[21] Bishop, D. E., and Mills, J. F., "Update of Aircraft Profile Data for the Integrated Noise Model Computer Program," Federal Aviation Administration, Mar. 1992.
[22] Sturdy, J. L., Andrews, J. W., and Welch, J. D., "Aircraft Trajectory Prediction for Terminal Automation," AIAA Guidance, Navigation, and Control Conference, Boston, AIAA Paper 1989-3634, Aug. 1989.
[23] Seah, C. E., and Hwang, I., "Stochastic Linear Hybrid Systems: Model and Estimation and Application to Air Traffic Control," *IEEE Transactions on Control Systems Technology*, 2007 (to be published).
[24] Householder, A. S., *The Theory of Matrices in Numerical Analysis*, Blaisdell, New York, 1965, p. 59.
[25] Genz, A., "Numerical Computation of Multivariate Normal Probabilities," *Journal of Computational and Graphical Statistics*, Vol. 1, 1992, pp. 141–149. doi:10.2307/1390838
[26] Cox, D. R., and Wermuth, N., "A Simple Approximation for Bivariate and Trivariate Normal Integrals," *International Statistical Review*, Vol. 59, No. 2, 1991, pp. 263–269. doi:10.2307/1403446
[27] Deak, I., "Probabilities of Simple *n*-Dimensional Sets for the Normal Distribution," *IIE Transactions*, Vol. 35, No. 3, Mar. 2003, pp. 285–293.
[28] Miwa, T., Hayter, A. J., and Kuriki, S., "The Evaluation of General Non-Centered Orthant Probabilities," *Journal of the Royal Statistical Society Series B (Methodological)*, Vol. 65, No. 1, Jan. 2003, pp. 223–234. doi:10.1111/1467-9868.00382
[29] Tong, Y. L., *The Multivariate Normal Distribution*, Springer–Verlag, New York, 1990, pp. 120–140.